nature geoscience

ARTICLES

PUBLISHED ONLINE: 10 JULY 2017 | DOI: 10.1038/NGEO2986

Reduced North American terrestrial primary productivity linked to anomalous Arctic warming

Jin-Soo Kim[1], Jong-Seong Kug[1]*, Su-Jong Jeong[2]*, Deborah N. Huntzinger[3], Anna M. Michalak[4], Christopher R. Schwalm[5,6], Yaxing Wei[7] and Kevin Schaefer[8]

Warming temperatures in the Northern Hemisphere have enhanced terrestrial productivity. Despite the warming trend, North America has experienced more frequent and more intense cold weather events during winters and springs. These events have been linked to anomalous Arctic warming since 1990, and may affect terrestrial processes. Here we analyse multiple observation data sets and numerical model simulations to evaluate links between Arctic temperatures and primary productivity in North America. We find that positive springtime temperature anomalies in the Arctic have led to negative anomalies in gross primary productivity over most of North America during the last three decades, which amount to a net productivity decline of 0.31 PgC yr^{-1} across the continent. This decline is mainly explained by two factors: severe cold conditions in northern North America and lower precipitation in the South Central United States. In addition, United States crop-yield data reveal that during years experiencing anomalous warming in the Arctic, yields declined by approximately 1 to 4% on average, with individual states experiencing declines of up to 20%. We conclude that the strengthening of Arctic warming anomalies in the past decades has remotely reduced productivity over North America.

Over the past few decades, changes in climate caused by anthropogenic forcings and natural feedback processes have affected terrestrial ecosystem productivity over the globe[1,2]. One of the main consequences of terrestrial ecosystem changes is an increase in terrestrial gross primary productivity (GPP), for example, expansion of shrub cover, enhanced vegetation photosynthesis and lengthening of the growing season, especially at high latitudes[3,4]. These positive changes in high-latitude vegetation productivity are closely related to the recent warming across high-latitude regions[5]. According to the observed records, the Arctic region shows a remarkable recent rapid temperature trend in comparison with other regions; this is termed as Arctic amplification[6–10]. However, it has been recently reported that anomalous Arctic warming can lead to severe cold events in mid-latitudes[6,11]. Although Arctic warming has resulted in positive changes in vegetation productivity at high latitudes, it is possible that it affects mid-latitude terrestrial ecosystems in the opposite way via remote teleconnections induced by anomalous Arctic warming. However, our understanding of the remote impacts of anomalous Arctic warming on terrestrial GPP in mid-latitudes is still insufficient.

Atmospheric teleconnections linked to Arctic warming

Recently, it was reported that regional Arctic temperature anomalies are critical to explaining climate variations in downstream regions; for example, the Arctic temperature anomalies over the East Siberian–Chukchi Sea are closely related to cold winters over North America via downstream teleconnection development[6,10]. To represent the regional Arctic temperature anomalies, we use the Arctic temperature (ART) index, which was introduced in a previous study[6], that averaged temperature anomalies over the East Siberian–Chukchi Sea (160° E–160° W, 65°–80° N). The March ART index (Supplementary Fig. 1) particularly shows the most significant relation with simultaneous and lagged temperature anomalies over North America (Supplementary Figs 2a and 3); thereby, this index is used for evaluating remote impacts of regional Arctic temperature anomalies on mid-latitude atmospheric conditions and terrestrial GPP over North America (see Methods).

We first examine the atmospheric teleconnection pattern related to Arctic temperature anomalies, which is represented by the regressed circulation pattern with respect to the ART index for the period 1979–2015. Figure 1a shows distinctive positive sea-level pressure anomalies over Alaska, which might be a direct response to positive temperature anomalies in the Arctic[6]. This anticyclonic flow induced by local forcing is expanded eastward because of strong low-level cold advection. In the upper level, a distinctive anticyclone located over Alaska shows an equivalent barotropic structure (Fig. 1b). In addition, cyclonic and anticyclonic anomalies are located in the downstream regions; this can be explained via Rossby wave propagation[12]. As a result of the anomalous Arctic warming-induced atmospheric teleconnection, low-level anticyclone and upper-level cyclone anomalies, which provide favourable conditions for severe cold weather, are developed over North America.

Consistent with the large-scale atmospheric pattern, considerable negative surface temperature anomalies are observed in northern North America, whereas Alaska and East Siberia show positive anomalies (Fig. 1c). In contrast to the northerly wind in northern North America, an anomalous southwesterly wind along the east coast of the United States is also observed, which is related to an anomalous anticyclone over the subtropical Atlantic. The anomalous southwesterlies indicate an eastward shift of the

[1]Division of Environmental Science and Engineering, Pohang University of Science and Technology (POSTECH), Pohang 37673, South Korea. [2]School of Environmental Science and Engineering, South University of Science and Technology of China (SUSTECH), Shenzhen 518055, China. [3]School of Earth Sciences and Environmental Sustainability, Northern Arizona University, Flagstaff, Arizona 86011, USA. [4]Department of Global Ecology, Carnegie Institution for Science, Stanford, California 94305, USA. [5]Woods Hole Research Center, Falmouth, Massachusetts 02540, USA. [6]Center for Ecosystem Science and Society, Northern Arizona University, Flagstaff, Arizona 86011, USA. [7]Environmental Sciences Division and Climate Change Science Institute, Oak Ridge National Laboratory, Oak Ridge, Tennessee 37831, USA. [8]National Snow and Ice Data Center, Cooperative Institute for Research in Environmental Sciences, University of Colorado at Boulder, Boulder, Colorado 80309, USA. *e-mail: jskug@postech.ac.kr; sujong@sustc.edu.cn

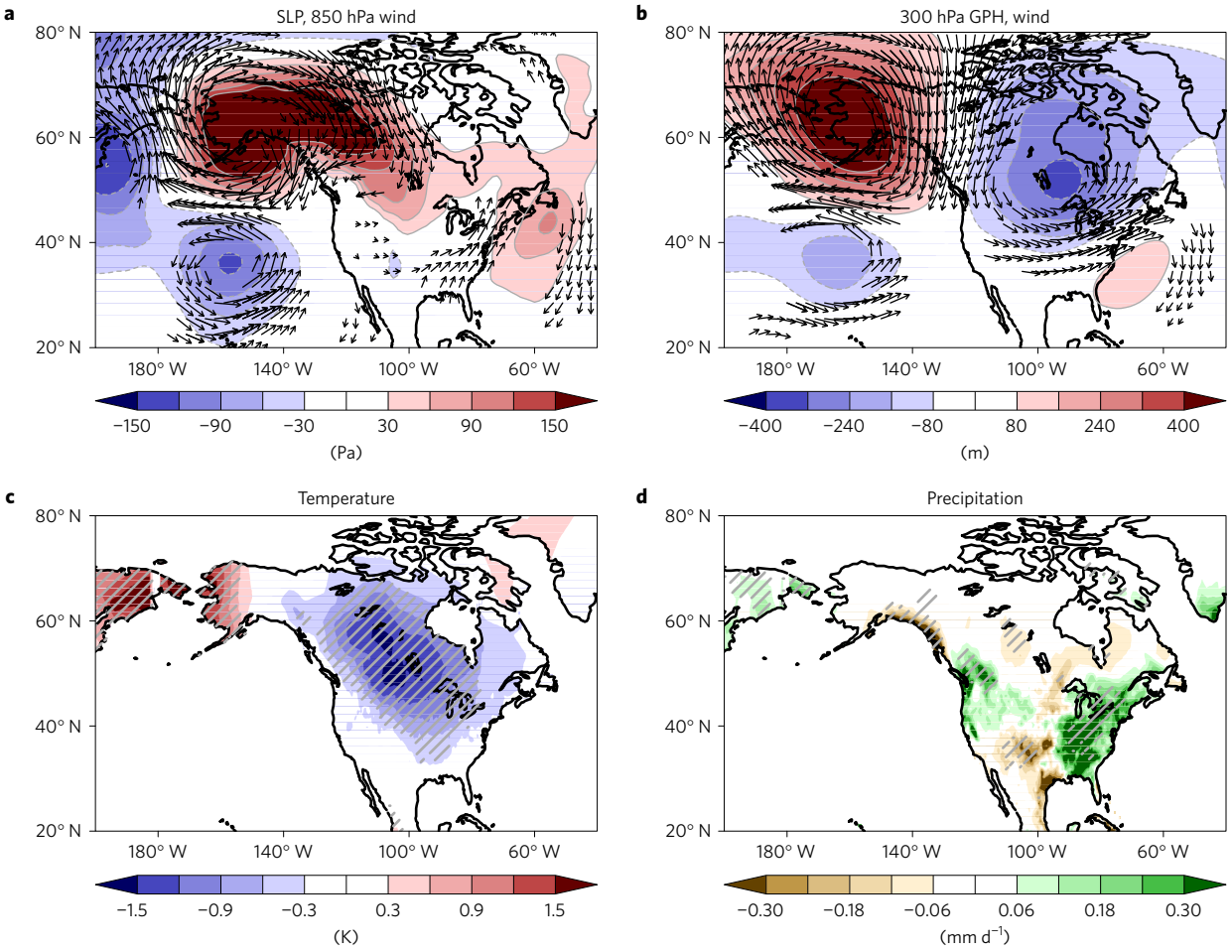

Figure 1 | Atmospheric teleconnections related to Arctic warming. a–d, Regression coefficients of the March–May mean sea-level pressure (SLP), 850-hPa wind (**a**), 300-hPa geopotential height (GPH) and wind (**b**), surface temperature (**c**) and precipitation (**d**) with respect to the ART index for the period 1979–2015. Wind vectors and hatching are displayed only in significant regions at the 95% confidence level (calculated using a Student's *t*-test).

Great Plains low-level jet, which can lead to a dipole precipitation pattern via alteration of moisture transport[13].

Terrestrial productivity anomalies linked to Arctic warming

As illustrated in Fig. 1, significant temperature and precipitation anomalies over North America are observed in association with Arctic temperature variation. It is expected that the changes in continental-scale anomalous temperature and precipitation over North America could affect terrestrial ecosystems. To examine the impact of Arctic warming on terrestrial GPP over North America, the relations of multiple data sets, as a proxy of terrestrial GPP, with the ART index are analysed. It is evident that negative vegetation activity and terrestrial GPP are captured across North America related to anomalous Arctic warming (Fig. 2, also Supplementary Fig. 4a,b). An extensive area of North America, from the boreal coniferous forests in Canada to the subtropical steppe in Mexico, exhibits significant changes in terrestrial GPP. It is clear that there is consistent vegetation activity in terms of spatial pattern among various data sets, for example, the satellite remote sensing of the normalized difference vegetation index (NDVI; Fig. 2a) for the period 1982–2013, and the flux tower data-driven GPP based on a model tree ensemble (MTE) for the period 1982–2011 (Fig. 2b). The terrestrial ecosystem models also show consistent results; that is, the simulated multi-model ensemble (MME) GPP is negatively correlated to the ART index (Fig. 2c). Although the trends of NDVI and GPP can be dependent on the data period[14], we found that anomalous Arctic warming-induced terrestrial productivity anomalies are not sensitive to data period (Supplementary Fig. 5). In addition, the Earth system models, which participated in the Coupled Model Intercomparison Project Phase 5 (CMIP5), show consistent results (Supplementary Fig. 6). Despite limited observed sample size, the observed GPP variations from individual flux towers show consistent results with the large-scale data in terms of negative GPP anomalies in the case of anomalous Arctic warming (Supplementary Fig. 7). Even though MTE tends to underestimate interannual variability[15], both the data- and process-driven GPP indicate a change of about $-0.31\,\mathrm{PgC\,yr^{-1}}$ over North America (125°–85° W, 30°–60° N) (Fig. 2d).

The cold surface over North America would be a major driver for the negative terrestrial GPP associated with anomalous Arctic warming. Because temperate and boreal regions are composed of temperature-limited ecosystems[16–18] (Supplementary Fig. 8), terrestrial GPP anomalies in the northern part of North America are closely related to anomalous Arctic warming-related local temperature anomalies, which are shown in Fig. 1c. This is consistent with a previous study, which demonstrated that the weakening positive trends in spring and summer vegetation greenness are related to springtime temperature variations in that region[16]. In detail, the maximum NDVI and GPP anomalies appear in the northeast United States, that is, Great Lakes Basin (Fig. 2a,b), while the temperature anomaly maximum is located to the northwest of Great Lakes Basin, at the Saskatchewan and Manitoba provinces in Canada (Fig. 1c). This may be attributed to GPP sensitivity differences to cold damage, that is, vegetation cold tolerance,

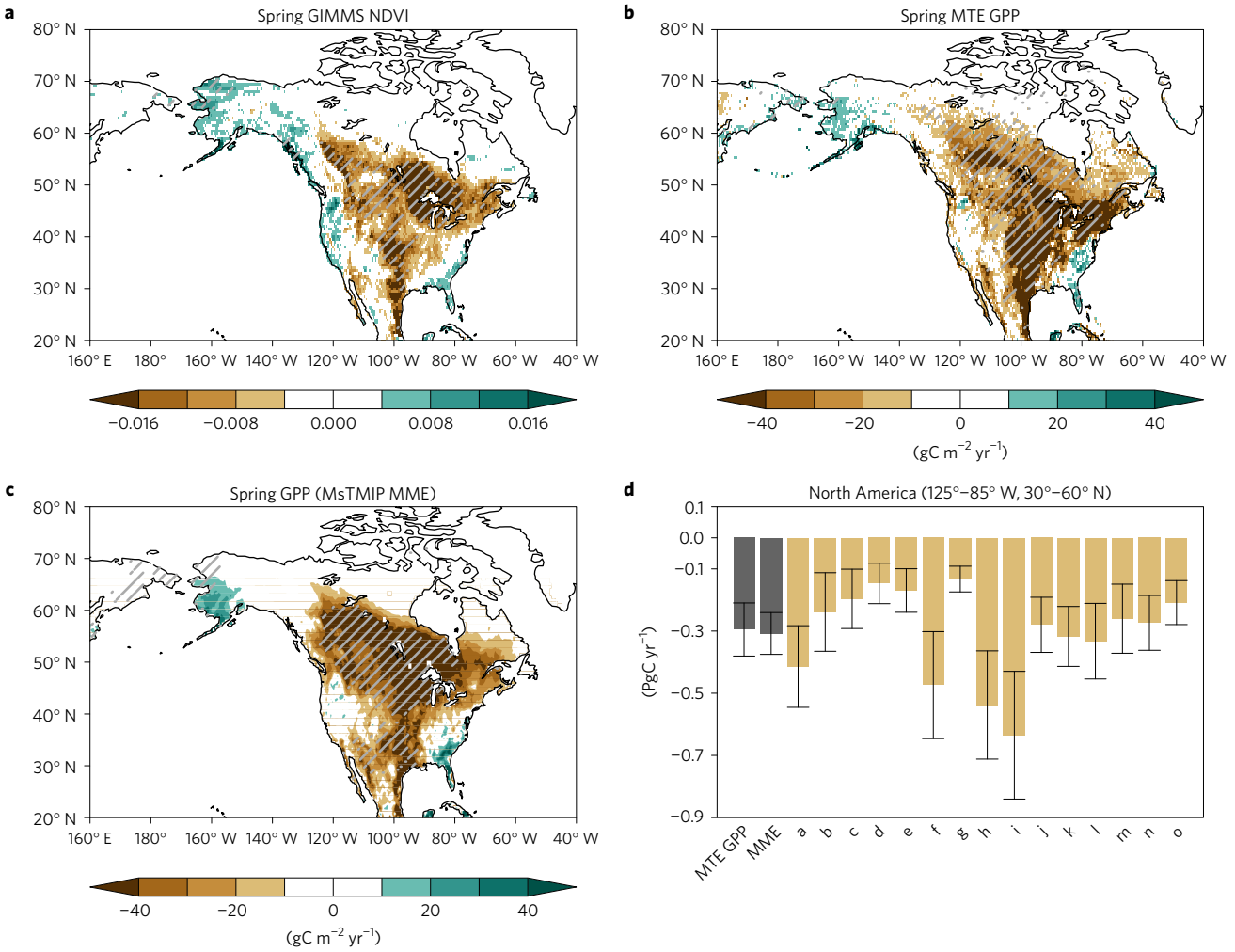

Figure 2 | Arctic warming impacts on spring terrestrial productivity. a–c, Regression coefficients of the spring (March–May) NDVI for the period 1982–2013 (**a**), flux tower data-driven GPP for the period 1982–2011 (**b**) and MME simulated GPP based on the MsTMIP for the period 1979–2010 (**c**) with respect to the ART index. **d**, Regression coefficient of the total GPP over North America (125°–85° W, 30°–60° N) with respect to the ART index based on MTE and MsTMIP (PgC yr^{-1}). Hatching and scale bars represent a range of 95% confidence level on the basis of a Student's *t*-test.

depending on plant functional types[18]. For example, the northern part of North America is comprised of a high fraction of evergreen needleleaf forest, which has relatively stronger cold tolerance than other land cover classes. However, deciduous broadleaf forest and mixed forest, which have higher GPP sensitivity to cold damage than evergreen needleleaf forest, are mainly distributed in Great Lakes Basin[18]; thereby, NDVI and GPP anomalies related to anomalous Arctic warming show a southeastward shift pattern as compared with temperature anomalies as shown in Fig. 1c.

In addition to the temperature effect, in the South Central United States, terrestrial variation might be related to precipitation anomalies with respect to anomalous Arctic warming, which are shown in Fig. 1d. Because of the water-limited ecosystems in that region[19], the terrestrial GPP reduction in the southern part of North America is mainly accompanied by a precipitation decrease in that region (Supplementary Fig. 8). In contrast to the decreased precipitation in the South Central United States, the increased precipitation on the east coast of the United States does not contribute to increased terrestrial GPP, because the ecosystems in that region are not water-limited (Supplementary Fig. 8b,d), possibly because of the presence of a sufficient amount of climatological precipitation.

Furthermore, in both the flux tower data-driven and simulated results, monthly GPP anomalies to March Arctic temperature anomalies show that the Arctic temperature-induced impacts on terrestrial GPP are maximum in May and even maintained until early summer (Fig. 3). Ecologically, environmental disturbances may lead to biological stresses, such as plant cellular dehydration, low stomatal conductance, suppressions of canopy development, and leaf area, especially for early spring, because newly emergent leaves in spring are sensitive to both cold[20] and drought[21] stresses due to lack of structural rigour, which is necessary to prevent cellular damage[22]. This is consistent with previous studies that argued changes in spring vegetation productivity tend to affect the productivity in terrestrial ecosystems over the following months[17,18]. In addition, annual mean NDVI and cumulative annual terrestrial GPP show significant anomalies over some parts of North America to spring local temperature and precipitation (Supplementary Fig. 9), suggesting spring atmospheric conditions have a role in interannual variability of terrestrial productivity in North America. Thus, abiotic stresses, such as cold and drought stresses, during spring from anomalous Arctic warming simultaneously suppress productivity and even contribute to reduction of annual productivity possibly by lasting effects on terrestrial ecosystem function[17,18,20,21].

Impacts on the United State crop yield

Consistent with cumulative annual terrestrial GPP, United States national-level crop-yield data reveal that annual yields of corn, soybeans and wheat in Arctic warming years as compared with

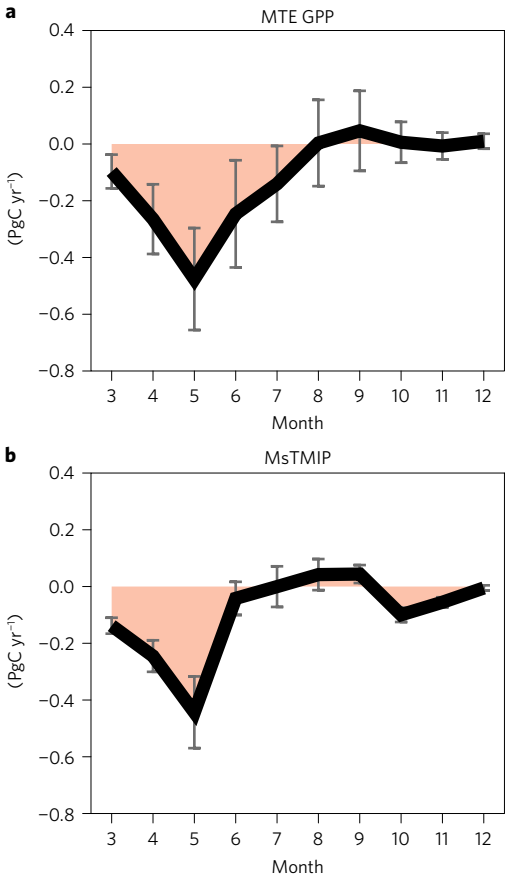

Figure 3 | Impacts of Arctic warming on monthly terrestrial productivity. **a**,**b**, Regression coefficients of monthly North American (125°–85° W, 30°–60° N) GPP in flux tower data-driven GPP (**a**) and MsTMIP (**b**). Error bars indicate 95% confidence levels.

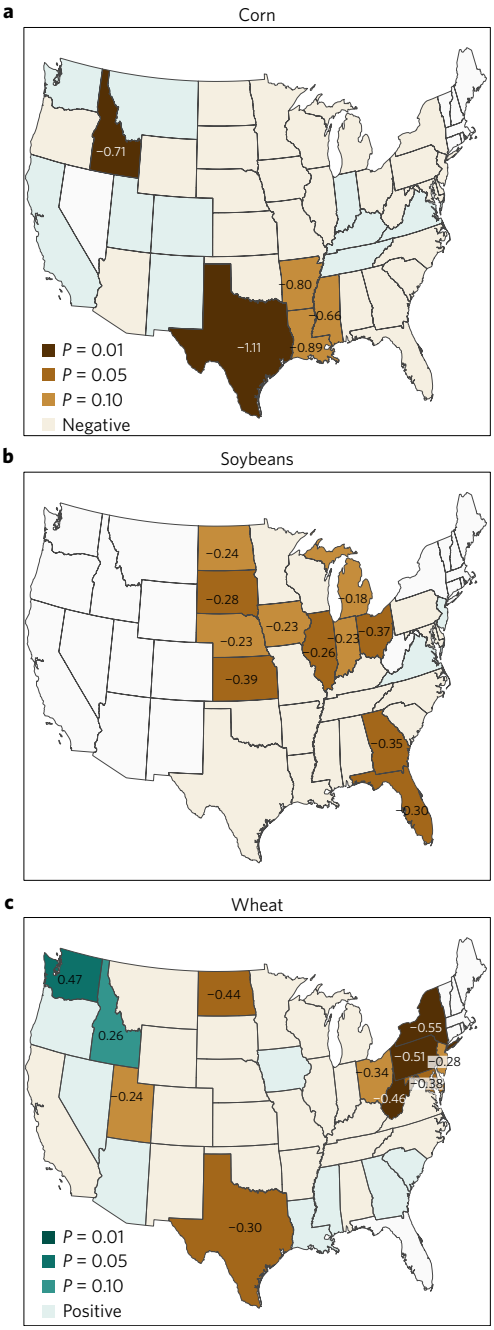

Figure 4 | Impacts of Arctic warming on United States crop yields. **a**–**c**, Statistical significance levels plotted as composite differences between the cases of Arctic warming and cooling for corn (**a**), soybeans (**b**) and wheat (**c**) on the basis of the bootstrap estimation. The numbers in each state denote composite differences in t ha^{-1} yr^{-1} only for $P < 0.1$. Light brown and green indicate non-significant states and white means undefined states due to the lack of crop-yield data.

Arctic cooling years declined by approximately 1.74, 3.96 and 3.62%, respectively. Figure 4 shows state-level crop-yield differences between Arctic warming and cooling cases, suggesting that all three major crops mainly exhibit negative changes in response to anomalous Arctic warming, albeit with some differences in crop fraction, crop sensitivity to climatic conditions, and management scheme between states[23]. The regions that display significantly reduced crop yields are consistent with the overall negative terrestrial productivity anomalies over North America that were obtained by remote sensing of NDVI and both of data- and process-driven GPP (Figs 2 and 4), even including irrigated cropland in the southern part of the United States. In all three crops, reduced crop yields are concurrently apparent in the Great Plains, such as in North Dakota (soybeans −0.24 and wheat −0.44 t ha^{-1} yr^{-1}), South Dakota, Nebraska and Kansas (soybean −0.39 t ha^{-1} yr^{-1}). The largest decrease in crop yields is observed in corn in the southern part of the United States, especially in Texas (−1.11 t ha^{-1} yr^{-1}; this value is approximately 20% of the productivity of a normal year in this region). As shown in the atmospheric responses to anomalous Arctic warming, the reductions in crop yield in the southern United States could be related to decreases in precipitation (Fig. 1d). This may be because crop productivity in dry areas of the southern United State is crucially dependent on water resources. In contrast to the southern part of the Great Plains, the decreasing crop yield in the northern part of the Great Plains might be related to spring temperature decreases. Although changes in crop yields related to anomalous Arctic warming show negative relations in most of the regions, a few states in the northwestern United States exhibit positive relations, especially for wheat yield. This pattern can be explained by precipitation increases in the northwestern United States (Fig. 1d), which may have a positive impact on wheat productivity[24].

Overall, the present study demonstrates for the first time an apparent linkage between Arctic temperature variations and agricultural productivity in mid-latitudes. As the understanding of large-scale circulation patterns can be useful to improve the predictability of terrestrial productivity and crop yields[25–29], our results suggest that Arctic information could be used to forecast agricultural productivity and reduce its uncertainty. In particular, because the interannual Arctic temperature variation has been

distinctly stronger in recent decades with the rapid decline in Arctic sea ice[6,11], this Arctic temperature variation may have a negative impact on human life both in the form of adverse weather conditions and reduction in agricultural productivity over North America. Moreover, the simulated MME net ecosystem exchange anomaly associated with anomalous Arctic warming is approximately $-0.1\,\mathrm{PgC\,yr^{-1}}$ (Supplementary Fig. 10), which is approximately 20% of the interannual standard deviation range in the North American carbon sink[30].

Current climate models tend to reasonably simulate the negative terrestrial GPP anomalies associated with anomalous Arctic warming over North America (Supplementary Fig. 4), although the detailed spatial pattern is different from the patterns as shown in Figs 2 and 3. Moreover, these negative GPP anomalies are also visible in future climate simulations (Supplementary Fig. 11), suggesting that the relationship is robust. Interestingly, the Arctic-related GPP anomalies become even stronger under future climatic conditions, especially in northwest North America. This is because the sensitivity of GPP anomalies to local temperature becomes stronger under greenhouse warming (Supplementary Fig. 12) and it is consistent with previous studies that argued enhanced phenological frost damage in a warming climate[31–34]. That is, the ecosystem in that region will be damaged more severely by Arctic-induced cold stress in a warmer climate. This result delivers important implications for climate adaptation, but further investigation is needed to obtain a general conclusion.

Methods

Methods, including statements of data availability and any associated accession codes and references, are available in the online version of this paper.

Received 17 November 2016; accepted 6 June 2017; published online 10 July 2017

References

1. Myneni, R. B., Keeling, C. D., Tucker, C. J., Asrar, G. & Nemani, R. R. Increased plant growth in the northern high latitudes from 1981 to 1991. *Nature* **386,** 698–702 (1997).
2. Zhu, Z. *et al*. Greening of the Earth and its drivers. *Nat. Clim. Change* **6,** 791–795 (2016).
3. Bhatt, U. S. *et al*. Circumpolar Arctic tundra vegetation change is linked to sea ice decline. *Earth Intract.* **14,** 1–20 (2010).
4. Hinzman, L. D. *et al*. Evidence and implications of recent climate change in northern Alaska and other arctic regions. *Clim. Change* **72,** 251–298 (2005).
5. Piao, S. *et al*. Net carbon dioxide losses of northern ecosystems in response to autumn warming. *Nature* **451,** 49–52 (2008).
6. Kug, J. S. *et al*. Two distinct influences of Arctic warming on cold winters over North America and East Asia. *Nat. Geosci.* **8,** 759–762 (2015).
7. Francis, J. A. & Vavrus, S. J. Evidence linking Arctic amplification to extreme weather in mid-latitudes. *Geophys. Res. Lett.* **39,** L06801 (2012).
8. Cohen, J. *et al*. Recent Arctic amplification and extreme mid-latitude weather. *Nat. Geosci.* **7,** 627–637 (2014).
9. Screen, J. A. & Simmonds, I. Amplified mid-latitude planetary waves favour particular regional weather extremes. *Nat. Clim. Change* **4,** 704–709 (2014).
10. Wallace, J. M., Held, I. M., Thompson, D. W., Trenberth, K. E. & Walsh, J. E. Global warming and winter weather. *Science* **343,** 729–730 (2014).
11. Kim, B. M. *et al*. Weakening of the stratospheric polar vortex by Arctic sea-ice loss. *Nat. Commun.* **5,** 4646 (2014).
12. Honda, M., Inoue, J. & Yamane, S. Influence of low Arctic sea-ice minima on anomalously cold Eurasian winters. *Geophys. Res. Lett.* **36,** L08707 (2009).
13. Higgins, R. W., Mo, K. C. & Yao, Y. Interannual variability of the US summer precipitation regime with emphasis on the southwestern monsoon. *J. Clim.* **11,** 2582–2606 (1998).
14. De Jong, R., Verbesselt, J., Zeileis, A. & Schaepman, M. E. Shifts in global vegetation activity trends. *Remote Sens.* **5,** 1117–1133 (2013).
15. Jung, M. *et al*. Global patterns of land-atmosphere fluxes of carbon dioxide, latent heat, and sensible heat derived from eddy covariance, satellite, and meteorological observations. *J. Geophys. Res.* **116,** G00J07 (2011).
16. Wang, X. H. *et al*. Spring temperature change and its implication in the change of vegetation growth in North America from 1982 to 2006. *Proc. Natl Acad. Sci. USA* **108,** 1240–1245 (2011).
17. Jeong, S. J., Medvigy, D., Shevliakova, E. & Malyshev, S. Uncertainties in terrestrial carbon budgets related to spring phenology. *J. Geophys. Res.* **117,** G01030 (2012).
18. Kim, Y., Kimball, J. S., Didan, K. & Henebry, G. M. Response of vegetation growth and productivity to spring climate indicators in the conterminous United States derived from satellite remote sensing data fusion. *Agr. Forest Meteorol.* **194,** 132–143 (2014).
19. Nemani, R. R. *et al*. Climate-driven increases in global terrestrial net primary production from 1982 to 1999. *Science* **300,** 1560–1563 (2003).
20. Hufkens, K. *et al*. Ecological impacts of a widespread frost event following early spring leaf-out. *Glob. Change Biol.* **18,** 2365–2377 (2012).
21. Noormets, A. *et al*. Drought during canopy development has lasting effect on annual carbon balance in a deciduous temperate forest. *New Phytol.* **179,** 818–828 (2008).
22. Menzel, A. & Fabian, P. Growing season extended in Europe. *Nature* **397,** 659 (1999).
23. Butler, E. E. & Huybers, P. Adaptation of US maize to temperature variations. *Nat. Clim. Change* **3,** 68–72 (2013).
24. Tack, J., Barkley, A. & Nalley, L. L. Effect of warming temperatures on US wheat yields. *Proc. Natl Acad. Sci. USA* **112,** 6931–6936 (2015).
25. Cane, M., Eshel, G. & Buckland, R. Forecasting Zimbabwean maize yield using eastern equatorial Pacific sea-surface temperature. *Nature* **370,** 204–205 (1994).
26. Kim, J. S., Kug, J. S., Yoon, J. H. & Jeong, S. J. Increased atmospheric CO_2 growth rate during El Niño driven by reduced terrestrial productivity in the CMIP5 ESMs. *J. Clim.* **29,** 8783–8805 (2016).
27. Hallett, T. B. *et al*. Why large-scale climate indices seem to predict ecological processes better than local weather. *Nature* **430,** 71–75 (2004).
28. Ciais, P. *et al*. Europe-wide reduction in primary productivity caused by the heat and drought in 2003. *Nature* **437,** 529–533 (2005).
29. Bastos, A. *et al*. European land CO_2 sink influenced by NAO and East-Atlantic Pattern coupling. *Nat. Commun.* **7,** 10315 (2016).
30. King, A. *et al*. North America's net terrestrial CO_2 exchange with the atmosphere 1990–2009. *Biogeosciences* **12,** 399–414 (2015).
31. Gu, L. *et al*. The 2007 eastern US spring freezes: increased cold damage in a warming world? *Bioscience* **58,** 253–262 (2008).
32. Rigby, J. R. & Porporato, A. Spring frost risk in a changing climate. *Geophys. Res. Lett.* **35,** L12703 (2008).
33. Augspurger, C. K. Spring 2007 warmth and frost: phenology, damage and refoliation in a temperate deciduous forest. *Funct. Ecol.* **23,** 1031–1039 (2009).
34. Augspurger, C. K. Reconstructing patterns of temperature, phenology, and frost damage over 124 years: spring damage risk is increasing. *Ecology* **94,** 41–50 (2013).

Acknowledgements

We acknowledge the World Climate Research Programme's Working Group on Coupled Modelling, which is responsible for CMIP, and we thank the climate modelling groups (listed in Supplementary Table 4) for producing and making available their model output. Funding for the Multi-scale synthesis and Terrestrial Model Intercomparison Project (MsTMIP; https://nacp.ornl.gov) activity was provided through NASA ROSES Grant no. NNX10AG01A. Data management support for preparing, documenting and distributing model driver and output data was performed by the Modeling and Synthesis Thematic Data Center at Oak Ridge National Laboratory (ORNL; http://nacp.ornl.gov), with funding through NASA ROSES Grant no. NNH10AN681. Finalized MsTMIP data products are archived at the ORNL DAAC (http://daac.ornl.gov). Funding for AmeriFlux data resources was provided by the US Department of Energy's Office of Science. The authors thank N. Mueller for his careful comments on the crop data analysis. J.-S.Kug and J.-S.Kim were supported by the Korean Meteorological Administration Research and Development Program under Grant KMIPA2015-2092 and National Research Foundation of Korea (NRF-2017R1A2B3011511). S.-J.J. was supported by the startup of South University of Science and Technology of China.

Author contributions

J.-S.Kim compiled the data, conducted analyses, prepared figures, and wrote the manuscript. J.-S.Kug and S.-J.J. designed the research and wrote the majority of the manuscript content. All of the authors discussed the study results and reviewed the manuscript. D.N.H., A.M.M., C.R.S., Y.W. and K.S. provide the MsTMIP data.

Additional information

Supplementary information is available in the online version of the paper. Reprints and permissions information is available online at www.nature.com/reprints. Publisher's note: Springer Nature remains neutral with regard to jurisdictional claims in published maps and institutional affiliations. Correspondence and requests for materials should be addressed to J.-S.Kug or S.-J.J.

Competing financial interests

The authors declare no competing financial interests.

Methods

Arctic temperature index. We define the ART index as the normalized surface temperature over the East Siberian–Chukchi Sea (160° E–160° W, 65°–80° N) on the basis of the observations derived from interpolated HadCRUT4 data hybridized with the University of Alabama in Huntsville satellite data[35] (http://www-users.york.ac.uk/~kdc3/papers/coverage2013/had4_short_uah_v2_0_0.nc.gz) for the period 1979–2015 (Supplementary Fig. 1). This region shows not only a relatively strong temperature trend in recent years, but also a significant relation with mid-latitude weather extreme events, especially over North America[6]. As suggested by a previous study[6], Arctic temperature variation over the East Siberian–Chukchi Sea is closely related to temperature anomalies over North America (125°–85° W, 30°–60° N), especially during boreal winter and spring (Supplementary Fig. 2). Furthermore, the April and May temperature anomalies over North America have a significant relation with March ART index, which means the impact of anomalous Arctic warming in March is not limited to March, but is found throughout spring. This might be attributed to significant lagged autocorrelation for the March ART index until May (Supplementary Table 1). Even though the ART index is based on the March surface temperature (Supplementary Fig. 3a), the sea-ice concentration shows a significant relationship with respect to the March ART index over the Bering Sea until the late spring (Supplementary Fig. 3b). Surface temperature anomalies in the Bering Sea are maintained even in late spring possibly because of the activation of air–ice–ocean interactions during the sea-ice extent retreat period after the March sea-ice extent maximum. These robust changes in Arctic air–ice–ocean conditions throughout the spring season can act as a long-lived teleconnection source to affect atmospheric circulation changes in mid-latitudes, as shown in Fig. 1 and Supplementary Fig. 4. Therefore, the March ART index has not only a simultaneous relation with temperature and GPP anomalies over North America but also a significant lagged relation as shown in Supplementary Figs 2 and 3. In this regard, we use the March ART index to determine the effects of spring terrestrial GPP on Arctic temperature variation.

Used data set to obtain ART-induced teleconnection. To estimate the ART-induced teleconnection pattern, data on the monthly sea-level pressure, geopotential height, and wind for 1979–2015 are obtained from the ERA (European Centre for Medium-Range Weather Forecasts Reanalysis)-Interim[36] (http://apps.ecmwf.int/datasets/data/interim-full-moda); monthly surface temperature and precipitation are quantified using Climatic Research Unit (CRU) TS3.23 for the period 1979–2014[37] (http://www.cru.uea.ac.uk).

Several data sets, as a proxy for terrestrial GPP, are used to obtain a robust relation between the ART index and terrestrial productivity anomalies (Supplementary Table 2). The NDVI data are the product of the Global Inventory Modeling and Mapping Studies (GIMMS) database, obtained from the Advanced Very High Resolution Radiometer remote-sensed observations[38]. The 8-km NDVI grids were re-gridded to a common 0.5° × 0.5° latitude/longitude grid for the period 1982–2013 (https://ecocast.arc.nasa.gov/data/pub/gimms/3g.v0). We also included eddy covariance flux-based GPP data[15], derived from a diagnostic model calibrated using global flux site-level data by means of a MTE machine learning technique as a largely independent observation-based terrestrial primary production data set. These data-driven GPP data are provided by the Max Planck Institute for biogeochemistry for the period 1982–2011[15]. In addition, the simulated GPP by the Multi-scale Synthesis and Terrestrial Model Intercomparison Project[39] (MsTMIP), involving 15 individual models based on BG1 and SG3 simulations (Supplementary Table 3), is employed in this study for the period 1979–2010 (http://nacp.ornl.gov). The offline model simulations are all driven with the same set of climate drivers, such as CRU and North American Regional Reanalysis[40]. The GPP anomalies over North America to anomalous Arctic warming in the MME of MsTMIP show a consistent result with the result based on data-driven GPP in terms of both spatial pattern and quantity of carbon flux amount, even though data-driven approaches were assessed for underestimation of interannual variability[15]. Indeed, GPP sensitivities to temperature based on MTE (Supplementary Figs 8c and 9c) are weaker than results from the MME of MsTMIP (Supplementary Figs 8e and 9e), but statistically significant especially in the boreal region. This result is consistent with a previous study, suggesting that terrestrial carbon cycle models show a close result with MTE in terms of GPP sensitivity to temperature anomalies, especially for the boreal region (48°–90° N), which is a temperature-limited region[41].

To examine anomalous Arctic warming impacts on agricultural production, United States crop-yield national and state-level data were downloaded for the period 1979–2015 from a web-accessible database called 'Quick Stats 2.0' provided by the National Agricultural Statistics Service of the United States Department of Agriculture[42] (http://www.nass.usda.gov/Quick_Stats).

Furthermore, the relationship between the ART indices and relevant impacts is investigated in each of the 25 coupled Earth System Models incorporated in the Coupled Model Intercomparison Project Phase 5[43] (http://cmip-pcmdi.llnl.gov/cmip5/data_portal.html). We use the data for the last 30 years in both the historical and Representative Concentration Pathway 4.5 scenarios in each model and re-gridded results into a common 2.5° × 2.5° latitude/longitude grid. Details of each model are listed in Supplementary Table 4.

To find more evidence of ART-induced terrestrial GPP changes, the observed GPP variations from individual flux towers were also used (Supplementary Fig. 7). Details of each site are listed in Supplementary Table 5.

Linear regression analysis. To estimate the ART-induced teleconnection and terrestrial impacts, linear regression is conducted with respect to the normalized ART index. To focus on interannual relation, linear trends from all data sets were firstly removed. Since each data set has a different period (Supplementary Table 2), the linear trend is estimated based on the available data period. For the linear regression, the linear trend of ART index is accordingly removed based on the same data period of the target data. The significance test conducted in this study is based on a standard two-tailed Student's t-test. As shown in Supplementary Figs 8, 9 and 13, we use a multiple regression to investigate the individual contributions of the temperature and precipitation anomalies to terrestrial GPP[41]. Consequently, the partial regression coefficients approximately represent the sensitivities of terrestrial GPP toward surface temperature and precipitation (see Supplementary Information).

Composite analysis. For crop-yield analysis, composite analysis is employed. Anomalous Arctic warming cases were defined when the ART index was $>0.75\sigma$, and cooling cases were defined when it was $<-0.75\sigma$ (Supplementary Fig. 1). To examine a significance of anomalous Arctic temperature variation impacts on each state of the United States, a bootstrap estimation is used for composite differences between anomalous Arctic warming and cooling cases. In the bootstrap method, to get the probabilistic density function, random resampling is repeated 10,000 times from the crop-yield data and the P value is determined from the histogram of random resampling (Fig. 4).

Data and code availability. The data (https://dx.doi.org/10.6084/m9.figshare.5053930) and code (https://dx.doi.org/10.6084/m9.figshare.5053948) that support the findings of the study are available in a persistent repository (http://figshare.com).

References

35. Cowtan, K. & Way, R. G. Coverage bias in the HadCRUT4 temperature series and its impact on recent temperature trends. *Q. J. R. Meteorol. Soc.* **140,** 1935–1944 (2014).
36. Dee, D. P. *et al*. The ERA-Interim reanalysis: configuration and performance of the data assimilation system. *Q. J. R. Meteorol. Soc.* **137,** 553–597 (2011).
37. Harris, I., Jones, P. D., Osborn, T. J. & Lister, D. H. Updated high-resolution grids of monthly climatic observations—the CRU TS3.10 Dataset. *Int. J. Climatol.* **34,** 623–642 (2014).
38. Tucker, C. J. *et al*. An extended AVHRR 8-km NDVI dataset compatible with MODIS and SPOT vegetation NDVI data. *Int. J. Remote Sens.* **26,** 4485–4498 (2005).
39. Huntzinger, D. N. *et al*. The North American Carbon Program Multi-scale synthesis and Terrestrial Model Intercomparison Project—Part 1: overview and experimental design. *Geosci. Model. Dev.* **6,** 2121–2133 (2013).
40. Wei, Y. *et al*. The North American Carbon Program Multi-scale synthesis and Terrestrial Model Intercomparison Project—Part 2: environmental driver data. *Geosci. Model. Dev.* **6,** 5375–5422 (2013).
41. Piao, S. *et al*. Evaluation of terrestrial carbon cycle models for their response to climate variability and to CO_2 trends. *Glob. Change Biol.* **19,** 2117–2132 (2013).
42. NASS quick stats, USDA National Agricultural Statistics Service (2008).
43. Taylor, K. E., Stouffer, R. J. & Meehl, G. A. An overview of CMIP5 and the experiment design. *Bull. Am. Meteorol. Soc.* **93,** 485–498 (2012).